PNAS RESEARCH ARTICLE | APPLIED PHYSICAL SCIENCES

High conductivity Sepia melanin ink films for environmentally benign printed electronics

Anthony Camus[a], Manuel Reali[a], Michael Rozel[b], Mariia Zhuldybina[b], Francesca Soavi[c], and Clara Santato[a,1]

Edited by Alberto Salleo, Stanford University, Stanford, CA; received January 7, 2022; accepted June 27, 2022 by Editorial Board Member Joanna Aizenberg

Melanins (from the Greek μέλας, mélas, black) are bio-pigments ubiquitous in flora and fauna. Eumelanin is an insoluble brown–black type of melanin, found in vertebrates and invertebrates alike, among which Sepia (cuttlefish) is noteworthy. Sepia melanin is a type of bio-sourced eumelanin that can readily be extracted from the ink sac of cuttlefish. Eumelanin features broadband optical absorption, metal-binding affinity and antioxidative and radical-scavenging properties. It is a prototype of benign material for sustainable organic electronics technologies. Here, we report on an electronic conductivity as high as 10^{-3} S cm^{-1} in flexographically printed Sepia melanin films; such values for the conductivity are typical for well-established high-performance organic electronic polymers but quite uncommon for bio-sourced organic materials. Our studies show the potential of bio-sourced materials for emerging electronic technologies with low human- and eco-toxicity.

bio-sourced materials | ink formulation | flexographic printing | electronic conductivity | percolation

Significance

Exclusive electronic transport over micrometric distances is uncommon in bio-sourced materials, usually featuring protonic or proton-assisted electronic transport. We found that films of Sepia melanin (the natural black–brown bio-pigment extracted from cuttlefish), flexographically printed from ink formulations including a binder, feature electronic conductivity as high as 10^{-3} S cm^{-1}, an outstanding value for natural materials. Sepia melanin features a hierarchical structure, including granules as one of the sub-unit levels. We hypothesize that the binder confines Sepia melanin granules, leading to the formation of continuous inter-granular paths for efficient charge carrier percolation. Implicitly, our results reveal the high intra-granular conductivity of Sepia melanin. By shedding light on the transport physics of natural materials, we pave the way toward sustainable organic electronic technologies.

Over a billion years of evolution, nature has provided us with a myriad of materials with incredibly different colors, structures, and responses to external stimuli such as thermal, mechanical, electrical, and photochemical.

Living foundries (i.e., flora and fauna) fabricate natural materials that constitute an immense source of inspiration for humanity. This is, for instance, the case in artificial photosynthesis that mimics the conversion of solar energy into chemical energy taking place in plants, through cascades of photo-induced electron transfers (1) or synthetic DNA data storage (2).

Nature could be the source of abundant and environmentally benign (sustainable) organic materials to be used in next-generation biodegradable electronics, paving a way toward a more sustainable use of resources. The ever-growing demand for electronic devices, combined with rapidly changing demand in consumer electronics to keep up with performance requirements, has unfortunately led to massive amounts of waste of electrical and electronic equipment (WEEE) that contain hazardous substances that pose major health and environmental concerns (3, 4). Further, modern electronic technology has an imbalanced product fabrication vs. exploitation consumed energy relationship: operationally energy-efficient devices have high embodied energy, expended in their production phase and stored in their constituents (5, 6).

A promising route to alleviate the environmental footprint of electronics is based on the use of abundant bio-sourced organic materials, novel production schemes involving solution processing (e.g., printing), nontoxic materials, and eco-design of devices that includes environmentally acceptable end-of-life scenarios (7–9).

Organic electronic materials based on conjugated organic molecules and polymers (that is, alternating single and double carbon bonds) develop from molecules or polymers through weak van der Waals interactions. The transition from individual molecules to materials through π–π stacking is paralleled by the generation of electronic bands from individual molecular energy levels, similarly to inorganic semiconductors (10–12). The work of Heeger, MacDiarmid, and Shirakawa on conductive polymers triggered enormous interest in organic electronics (13). Organic thin-film transistors and organic solar cells have been intensively investigated in the past 2 decades (14). Nowadays, organic light-emitting diodes can be found in mobile phones and TV displays.

Sustainable (green) organic electronics is not meant to replace silicon in high performance electronics. It may complement silicon and extend its capabilities in emerging areas where low eco- (and human-) toxicity, mechanical flexibility, and low production costs are important such as smart wearables, fieldable environmental sensors, food monitoring, and consumer electronics.

Eumelanin is a prototype of benign material for sustainable organic electronic technologies and their powering elements (15–17). The bio-pigment features diverse

Author contributions: A.C., M. Reali, and C.S. designed research; A.C., M. Reali, M. Rozel, M.Z., and C.S. performed research; A.C., M. Reali, M. Rozel, and C.S. contributed new reagents/analytic tools; A.C., M. Reali, F.S., and C.S. analyzed data; and A.C., M. Reali, M. Rozel, F.S., and C.S. wrote the paper.

The authors declare no competing interest.

This article is a PNAS Direct Submission. A.S. is a guest editor invited by the Editorial Board.

[1]To whom correspondence may be addressed. Email: clara.santato@polymtl.ca.

This article contains supporting information online at http://www.pnas.org/lookup/suppl/doi:10.1073/pnas.2200058119/-/DCSupplemental.

Published August 1, 2022.

functions including photoprotection, antioxidant behavior, metal chelation and free-radical scavenging. Sepia melanin is a natural eumelanin extracted from the ink sac of cuttlefish.

Eumelanin is made up of redox-active and electronically conjugated (5, 6)-dihydroxyindole (DHI) and (5, 6)-dihydroxyindole-2-carboxylic acid (DHICA) building blocks (SI Appendix, Scheme S1 *A* and *B*), featuring several competing polymerization sites (18). As a result, eumelanin is a chemically disordered (heterogeneous) macromolecule (19). The chemical disorder leads to polymorphic π–π stacked regions in the supramolecular structure, such that eumelanin exhibits structural (and consequently energetic) disorder, at least in the short range (20–22). Importantly, hierarchical development characterizes the formation of eumelanin-based materials. Ensembles of oligomers of the two DHI and DHICA building blocks hierarchically build up via π−π stacking with an interplanar distance of ∼3.4 Å and lateral extension of ∼20 Å (20, 23, 24). Large particles, of 100–200 nm, form through further aggregation by π–π stacking and edge-to-edge H-bonding interactions. Such large particles can be tentatively associated to granules observable by transmission electron microscopy (TEM) images obtained from Sepia melanin samples (25). Sepia melanin-based ink formulations for applications in large-area printing of sustainable organic electronics are expected to preserve the integrity of Sepia melanin granules, while enabling its solution processability.

In the 1970s, McGinness et al. (26) reported on the reversible electrical resistive switching from a high (OFF) to a low (ON) resistive state in wet eumelanin-pressed pellets, interpreted within the amorphous semiconductor model (ASM). A crucial element in this work was the observation that hydrated pellets exhibited electrical resistive switching but dry pellets did not. This difference was explained using the modified dielectric constant theory, which posits that the adsorbed water increases the dielectric constant of the material, lowering the activation energy for charge-transfer processes (27). Reports on the electrical response of hydrated eumelanin pellets questioned the ASM and proposed a mixed ionic-electronic conductor model (28–33). Recently, we have observed predominant electronic transport in dry pellets of Sepia melanin (34). Transport has not previously been studied under the lens of eumelanin's hierarchical structure and its implications when probed at different lengths. At present, we lack a complete picture of the transport physics of eumelanin.

Here, we report on high electronic conductivity (as high as 10^{-3} S cm^{-1}, the state-of-the-art electrical conductivity of dry and highly hydrated eumelanin being 10^{-13} S cm^{-1} and 10^{-4} S cm^{-1}, respectively) in printed and spin-coated films from the bio-pigment Sepia melanin-formulated ink without any thermal or hydration treatment (35–37). As a term of comparison, well-established synthetic organic semiconductors typically feature conductivities within the range 10^{-4}–1 S cm^{-1}.

The ink, optimized for large scale roll-to-roll printing, includes the Sepia melanin bio-pigment and the insulating polymer binder polyvinyl butyral (PVB) (*SI Appendix*, Scheme S1 *C*), commonly used in ink formulation processes to stabilize insoluble pigments in the ink state and improve the rheological and adhesion properties of the ink upon printing. The use of low toxicity components, well-established in the printing industry, opens the opportunity to scale up the production of Sepia melanin ink and the fabrication of sustainable organic electronic devices based thereon.

We propose that, in our films, the presence of the insulating binder improves the contacts among the Sepia melanin granules, thus affecting the transport properties at their interfaces, eventually leading to intergranular percolation phenomena. In our hypothesis, the binder enables the transition from intragranular (nanometric scale) to intergranular (micrometric scale) transport.

Results

Sepia Melanin Ink Formulations and Processing. Sepia melanin ink was prepared by dispersing Sepia melanin powders, extracted, and purified from the ink sac of cuttlefish, in a predissolved mix of PVB (binder) and 1-propanol (Fig. 1 *A* and *B*). To homogenize the ink, the mix was mechanically processed at high rotational speed in a water-cooled vessel with zirconium oxide beads (Fig. 1*B*). 1-Methoxy-2-propanol and TEGO Wet KL 245 (polyether siloxane copolymer-based surfactant) were added during mixing to decrease the evaporation rate and improve the surface wetting properties of the ink for roll-to-roll flexographic printing (Table 1 and *Materials and Methods*). The ink can be spin-coated onto silicon dioxide/silicon (SiO_2/Si) and flexographically printed into films (from now on referred to as Sepia melanin films) on polyethylene terephthalate (PET) and Kromekote paper (Fig. 1 *C* and *D*).

The height profiles of Sepia melanin films show that film thickness is approximately 1 μm and 3 μm for printed (on PET) and spin-coated films (on SiO_2/Si), respectively (*Materials and Methods* and SI Appendix, Fig. S1 and Table S1).

Scanning electron microscopy (SEM) images of spin-coated (on SiO_2/Si, Fig. 2 *A* and *B*) and printed films (on Kromekote paper, Fig. 2 *C* and *D*) show complete substrate coverage. The morphology by SEM of Sepia melanin films printed and spin-coated on paper and SiO_2/Si, respectively, comprises aggregates of PVB enclosing Sepia melanin granules in a matrix-like fashion (Fig. 2 *B* and *D*). The contact at the boundaries of Sepia melanin granules is significantly larger in the film state than in the powder state (SI Appendix, Fig. S2). Such an improved contact between Sepia granules is likely the consequence of the confining action of PVB (Fig. 1*E*).

Atomic force microscopy (AFM) images of Sepia melanin films spin-coated on SiO_2/Si reveal the presence of intragranular structures differing by adhesion properties likely attributable to several functional groups (red arrows, SI Appendix, Fig. S3).

Electrical Characterization of Sepia Melanin Films. Current–voltage (I–V) characteristics of Sepia melanin films spin-coated and printed onto Au-patterned SiO_2/Si and Ag-patterned PET and paper electrodes, respectively, show that the current is an increasing function of the voltage from 0 V to 10 V (Fig. 3 *A* and *B* and *Materials and Methods*). The electrical conductivity (σ) of Sepia melanin films spin-coated on SiO_2/Si, deduced using the four-point probe method (38), is $\sim 10^{-3}$ S cm^{-1} (see *Materials and Methods* and *SI Appendix*, Table S1).

These values are unprecedented for eumelanin films solution-processed at ambient conditions without any thermal or hydration treatment and for other organic electronic materials extracted from natural sources (28, 30, 35–37, 39–41).

I–V scans, sequentially measured for increasing voltage scan rates included between 5 and 500 mV s^{-1}, overlap (Fig. 3*A*). The independence of the I–V response on the rate points to a predominant electronic conduction in Sepia melanin films spin-coated on Au-patterned SiO_2/Si.

I–V characteristics at low voltage (i.e., from 0 V to 3 V) are linear (Ohmic) whereas at higher voltages (i.e., from 3 V to 10 V) they follow a power law of the type $I \propto V^a$ (non-Ohmic, $a \geq 1$) (Fig. 3 *A* and *B*). Our log(J)–log(V) scans, with J being

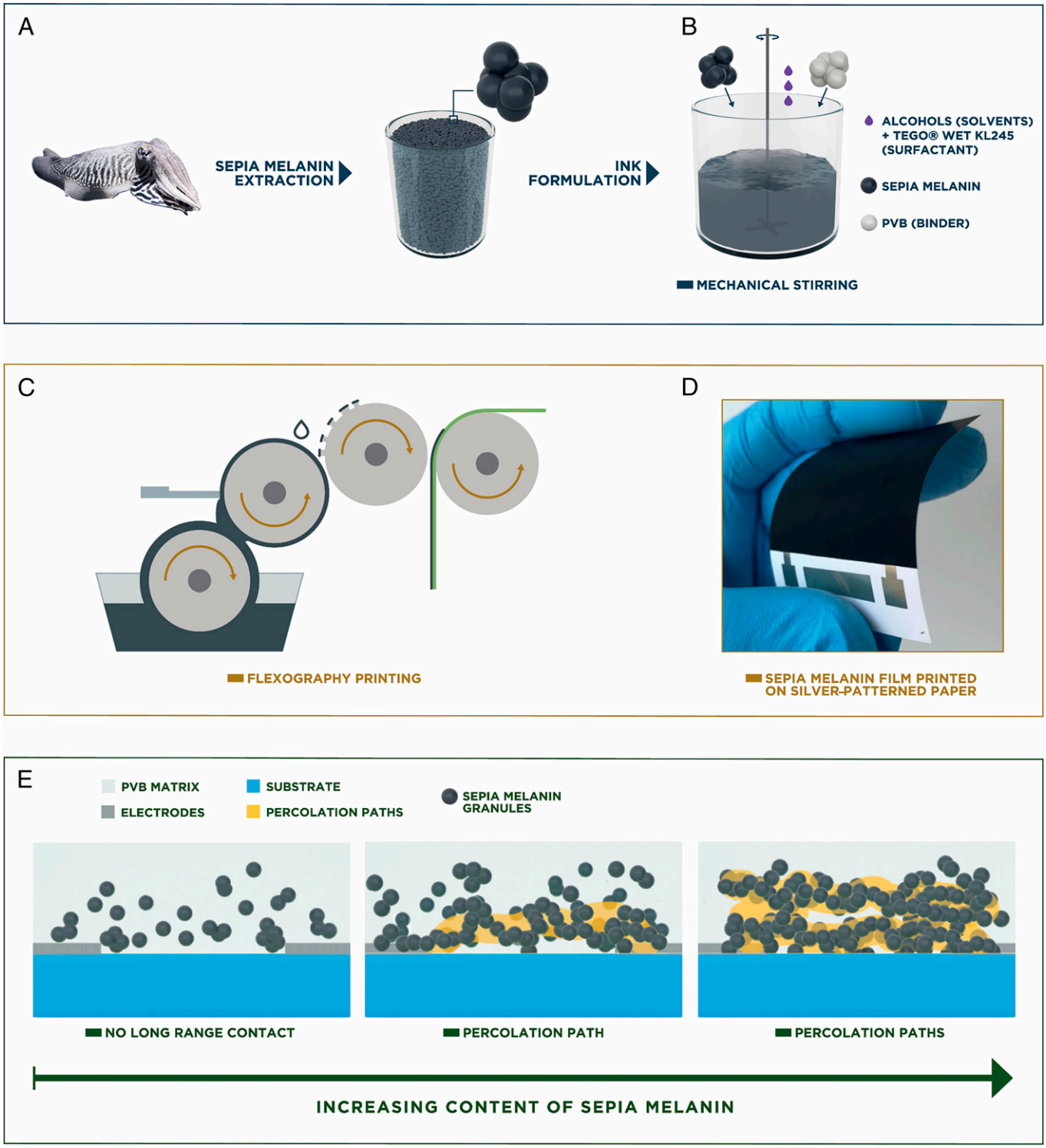

Fig. 1. Schematic of Sepia melanin (*A*) extraction and purification from the raw ink of cuttlefish, (*B*) ink formulation process, and (*C*) flexography printing. (*D*) Optical image of a printed Sepia melanin film onto Ag-patterned Kromekote paper (see *Materials and Methods*). (*E*) Schematic representation of the confining action of PVB and percolation phenomena taking place in spin-coated Sepia melanin films.

the current density, confirm a change of slope from an Ohmic regime ($a \pm \Delta a = 1.000 \pm 0.014$) to a non-Ohmic one ($a \pm \Delta a = 1.419 \pm 0.002$) (*SI Appendix*, Fig. S4).

The occurrence of this type of an I–V power law suggests the build-up of electronic space-charge layers at the Sepia melanin film/metal contact interface under the action of the electric field, as we previously reported for dry Sepia melanin pellets (34) and for DHI- and DHICA-eumelanin films (42). The formation of space-charge layers under electrical bias conditions is expected in organic materials because structural (physical) disorder produces electronic trap-states (43–45).

The current-time characteristics of Sepia melanin films spin-coated on Au-patterned SiO_2/Si show a plateau-like behavior indicating a prevalent electronic transport in Sepia melanin films, quite uncommon in bio-materials (Fig. 3*C*). In the case of mixed electronic-ionic (protonic) transport, the current-time

Table 1. Sepia melanin ink formulation prepared by using natural Sepia melanin powders extracted and purified from the ink sac of cuttlefish *Sepia officinalis* (see *Materials and Methods*)

Material (type)	Weight (g)	Weight (% wt/wt)
1-Propanol (solvent)	382.4	64.8
Polyvinyl butyral B-30HH (binder)	67.5	11.4
Sepia melanin powders (bio-pigment)	112.5	19.1
1-Methoxy-2-propanol (solvent)	26.0	4.4
TEGO Wet KL245 (surfactant)	1.5	0.3

characteristics would fit an exponential decay function, attributable to the formation of ionic double layers at the film/metal interface, followed by a plateau ascribable to electronic transport (35, 39).

To shed light on the nature of charge transfer and charge carrier transport processes, we collected impedance spectroscopy characteristics (IS) (see *Materials and Methods* and *SI Appendix, Text, IS section*) (46, 47). Nyquist plot (i.e., the negative imaginary part of the impedance [-Im (Z)]) as a function of the real part (Re [Z]), exhibits a single semicircle whose diameter is attributable to the electronic resistance of the Sepia melanin film (Fig. 3*D* and *SI Appendix*, Table S2). The presence of multiple semicircles would have been attributable to mixed electronic-ionic impedance. The absence of a low frequency capacitive tail suggests the absence of ion transport and accumulation at the Sepia melanin/Au electrodes (34, 47).

We can exclude an explanation of the electrical response as due to contamination (neutron activation analysis [NAA], *SI Appendix*, Table S3; UV-Vis-NIR absorption, *SI Appendix*, Fig. S5; Fourier transform infrared spectroscopy [FT-IR], *SI Appendix*, Fig. S6*A* and Table S4; Raman, *SI Appendix*, Fig. S6*B* and Table S5; X-ray photoelectron spectroscopy [XPS], *SI Appendix*, Fig. S7 and *Text*) (48–52).

We observe that the I–V response and current-time (I–t) characteristics of Sepia melanin films spin-coated on Au-patterned SiO_2/Si change as a function of the temperature (T). Increasing the temperature from 265 K to 325 K brings about an increase of the current intensity, I (Fig. 4 *A* and *B* and *SI Appendix*, Fig. S8*A* and Table S6) of the form $I = I_0 + sT$, where I_0 is the intercept and s the slope (*SI Appendix*, Fig. S8*B* and Table S7). From the linear fit, we estimate an increasing rate of the current with T of ~38 μA K^{-1}. The log (σ)-T^{-1} plot of Sepia melanin films spin-coated on Au-patterned SiO_2/Si fits the Arrhenius law with an activation energy for hopping $E_a = 26 \pm 2$ meV (*SI Appendix*, Fig. S8*C*). Such a temperature-dependent electrical response is compatible with the occurrence of thermally activated (electronic) hopping processes, these latter being extensively reported in organic semiconductors (26, 36, 53, 54). The abovementioned electrical properties pertain to Sepia melanin films featuring relative mass percentage of Sepia melanin to PVB of 62 wt% Sepia (38 wt% PVB). To shed light on the confining action of the insulating binder and its impact on the transport properties of Sepia melanin films, we formulated inks featuring several relative mass percentages (%wt/wt) of Sepia melanin to PVB (Fig. 5 and *SI Appendix*, Fig. S9*A*). The presence of the surfactant seems not to affect the electrical behavior of Sepia melanin films (*SI Appendix*, Fig. S9*B*). The plot logarithm of electrical conductivity vs. Sepia melanin content features an S-shape (Fig. 5). Remarkably, the electrical conductivity is ~10^{-12} S cm^{-1} and ~10^{-3} S cm^{-1} for films spin-coated on Au-patterned SiO_2/Si

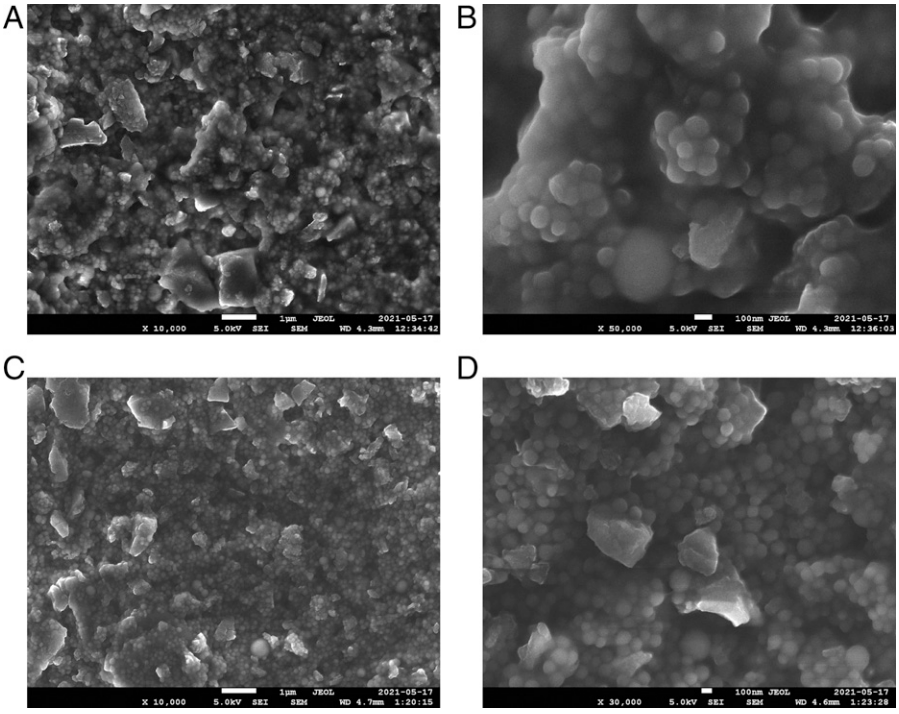

Fig. 2. SEM images of Sepia melanin films, (*A*) and (*B*) spin-coated on SiO_2/Si, (*C*) and (*D*) flexographically printed on paper. Scale bars: 1 μm in (*A*) and (*C*); 100 nm in (*B*) and (*D*).

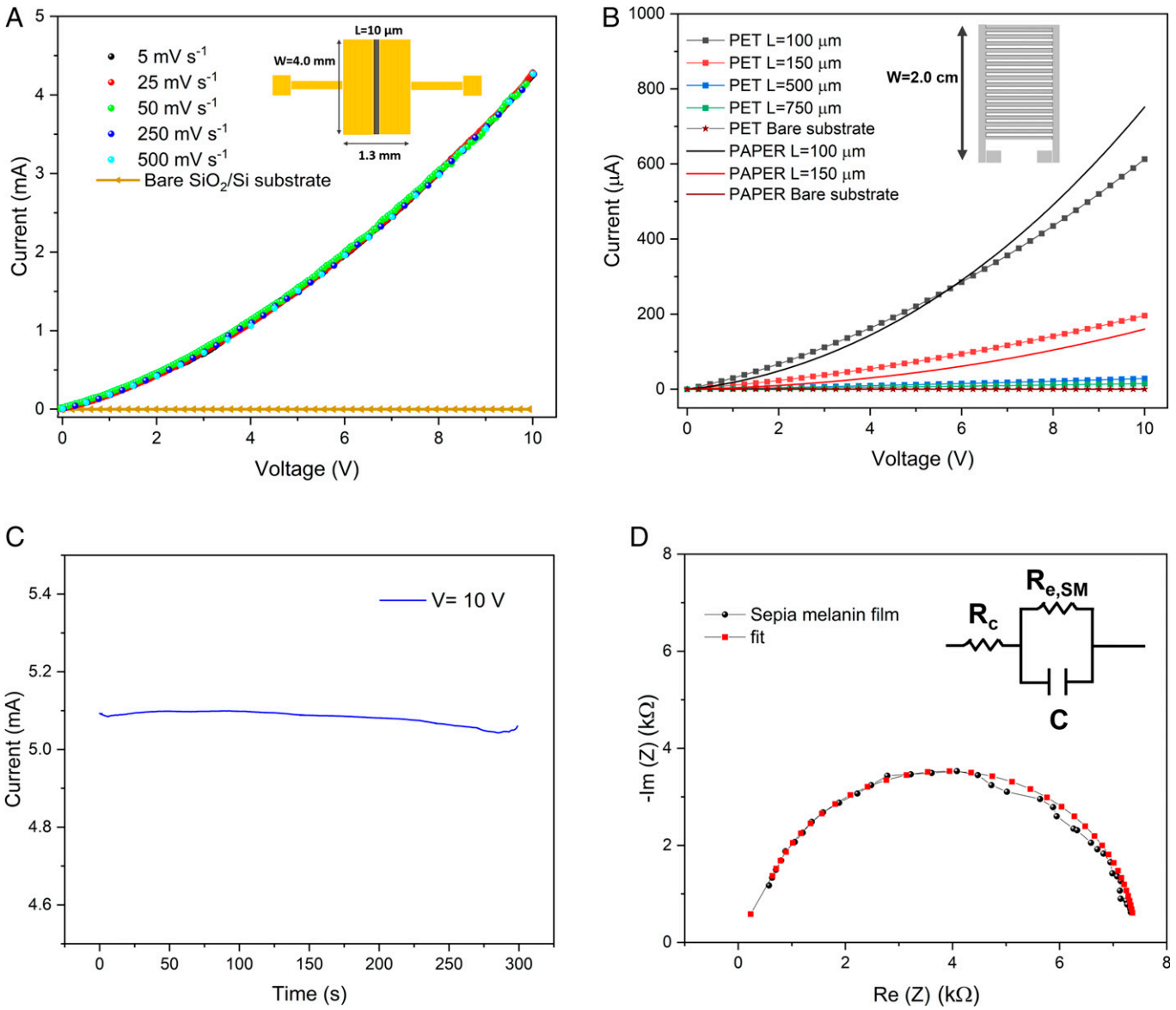

Fig. 3. Current-voltage response of Sepia melanin films spin-coated from Sepia melanin ink on (*A*) Au-patterned SiO_2/Si (planar configuration, see *Materials and Methods*), printed on (*B*) PET and paper substrates patterned with Ag printed electrodes (interdigitated configuration, see *Materials and Methods*); (*C*) current-time characteristics and (*D*) Nyquist plot of spin-coated Sepia melanin films on Au-patterned SiO_2/Si. (*A* and *B, Insets*) The electrode geometry on SiO_2/Si and PET and paper substrates, respectively. (*D*, *Inset*) The equivalent circuit used to fit the Nyquist plot. R_c is the Sepia melanin/Au electrodes resistance, $R_{e,SM}$ the Sepia melanin film resistance, and C the space charge capacitance (see SI Appendix, *Text, IS section*).

from inks featuring 9 wt% Sepia (91 wt% PVB) and 62 wt% Sepia (38 wt% PVB) ratios, respectively. SEM cross-section and topographic images of Sepia melanin films spin-coated on Au-patterned SiO_2/Si reveal that the extension and density of clusters of Sepia melanin granules considerably increase with the increase of Sepia melanin to PVB wt% (Fig. 5 and *SI Appendix*, Fig. S9).

These observations suggest the occurrence of a transition from a low electrical conductivity state to a high electrical conductivity state of Sepia melanin films spin-coated onto Au-patterned SiO_2/Si. The concentration threshold at which the insulating-to-conducting transition takes place can be interpreted as a percolation threshold that we located between 40 and 50 wt% of Sepia melanin (Fig. 5 and *SI Appendix*, Fig. S9). While this S-shape characteristics can be associated to percolation (55, 56) more experimental points are required to test and validate statistically a quantitative model of the observed phenomenon. Markedly, our findings suggest that beyond the concentration threshold, the gradual improvement of mutual contact of Sepia melanin granules enables long-range charge carrier transport.

Discussion

Here, we provided proof-of-concept printability of insoluble Sepia melanin bio-pigment, a prototype of benign material for sustainable technologies in environmentally benign electronics, by means of a low-toxicity, room-temperature ink formulation protocol. We successfully printed (flexography) and spin-coated Sepia melanin films on technologically relevant substrates (e.g., flexible PET and paper, SiO_2/Si).

Spin-coated and printed films feature record electronic conductivity of $\sim 10^{-3}$ S cm^{-1}, an outstanding value for bio-sourced materials. The I–V response, current-time characteristics and IS of Sepia melanin films spin-coated on Au-patterned SiO_2/Si point to predominant electronic transport (likely

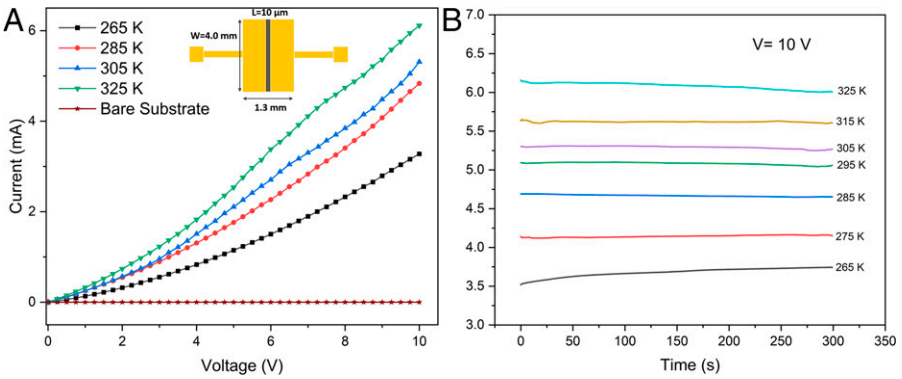

Fig. 4. Temperature-dependent (*A*) current-voltage response and (*B*) current-time characteristics of Sepia melanin films spin-coated from Sepia melanin ink on Au-patterned SiO_2/Si electrodes (planar configuration, see *Materials and Methods*). In (*A*), the electrical response of the bare Au-patterned SiO_2/Si electrodes has been acquired at 295 K and the *Inset* shows the electrode geometry.

enabled by molecular π–π stacking) with formation of space-charge layers. Remarkably, the electrical conductivity of Sepia melanin films spin-coated onto Au-patterned SiO_2/Si depends on Sepia melanin (active material) to PVB (binder) mass ratio. Indeed, we found a concentration threshold from low to high electrical conductivity between 40 and 50 wt% of Sepia melanin. Beyond this threshold, the electrical conductivity exponentially increases with the increase of the amount of Sepia melanin. SEM images reveal that the increase of Sepia melanin content brings about a significant decrease in the physical distance between clusters of Sepia melanin granules. We propose that the improved contact at the boundaries between Sepia melanin granules leads to the formation of continuous intergranular paths for electronic charge carrier transport, implicitly suggesting efficient intragranular transport.

Our results pave the way toward the exploitation of bio-sourced materials for high-performance, low-cost sustainable organic electronic technologies based on printed organic semiconductors.

Materials and Methods

Materials for Sepia Melanin Extraction. *Sepia officinalis* cuttlefish ink (Star-eef Seafood Boston, product of Spain) was purchased in a Montreal fish market. HCl (ACS Reagent 37%) was purchased from Acros Organics. Monobasic sodium phosphate, dibasic sodium phosphate solution (0.5 M in H_2O), ethanol (ACS reagent 99.8%), ethyl acetate, 1-propanol (≥99.5%) and 1-methoxy-2-propanol (≥99.5%) were purchased from Sigma-Aldrich. Polyvinyl butyral (PVB) B-30HH (molecular weight ∼33,000 g mol^{-1}) was purchased from MOWITAL. TEGO Wet KL 245 polyether siloxane copolymer additive was purchased from Evonik, whereas zirconium oxide beads (diameter, 1 mm; density, 5.5 g cm^{-3}) were purchased from Next Advance Inc.

Sepia Melanin Powders Extraction and Purification. Sepia melanin powders were extracted from the raw ink of *Sepia officinalis* using a protocol adapted from previously reported extraction procedures (34, 57–59). Briefly, 300 g of cuttlefish ink were suspended in 500 mL of HCl 2 M and stirred for 24 h at RT. After stirring, the slurry was centrifuged (Allegra-X30R Centrifuge, Beckman Coulter) and sequentially washed three times with 0.5 M HCl, once with de-ionized (DI) water and once in a buffer solution (0.02% vol/vol of monobasic sodium phosphate 200 mM, 32.49% vol/vol of dibasic sodium phosphate 200 mM, and 67.49% vol/vol of DI water), ethanol, DI water, and ethyl acetate. Finally, the slurry was washed four times with DI water. Each centrifugation step was performed at 10,000 rpm at 5 °C (15 min for HCl 2M, HCl 0.5 M ethanol and ethyl acetate, 25 min for the buffer solution and DI water). The final product was lyophilized at −80 °C for 24 h to remove residual DI water. Fine black Sepia melanin powders were obtained. This procedure provided an extraction yield from ∼10 to 12% in weight (e.g., ∼30–35 g of powder was obtained from 300 g of cuttlefish ink).

Ink Formulation and Printing. First, 67.5 g of PVB B-30HH were dissolved in 382.4 g of 1-propanol (73.2% wt/wt of the Sepia melanin ink formulation) (Table 1). The blend was then mixed in a high-rotation-speed disperser (1.5 hp, Engineered

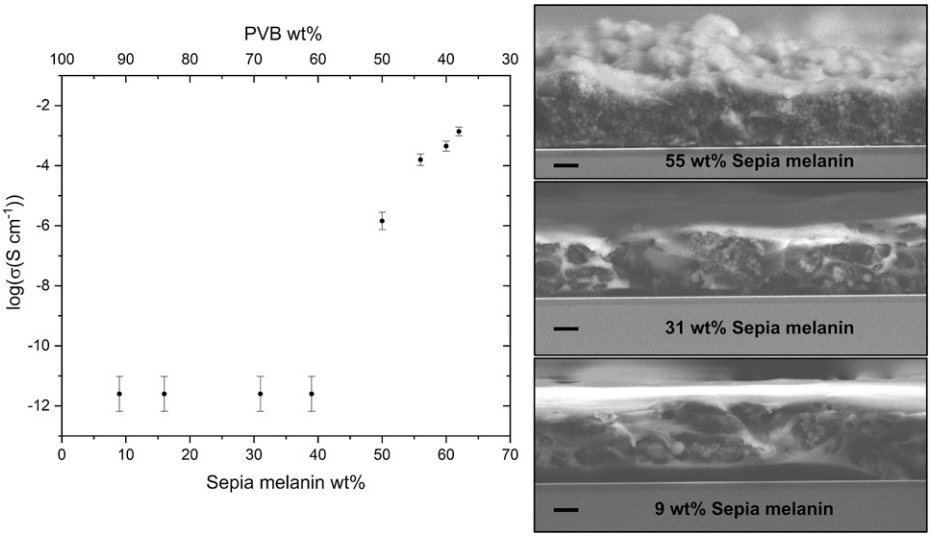

Fig. 5. Logarithm of the electrical conductivity of films spin-coated from Sepia melanin inks featuring different Sepia melanin to PVB wt% ratios on Au-patterned SiO_2/Si electrodes (see *Materials and Methods*). On the right, SEM cross-section images of 55 wt% (45 wt% PVB), 31 wt% (69 wt% PVB), and 9 wt% (91 wt% PVB) Sepia melanin films (*Top* to *Bottom*, respectively). (Scale bar: 1 µm.)

Mills Inc.) at 600 rpm for 20 min. Next, 112.5 g of manually grinded Sepia melanin powders were gradually added to the blend and mixed at 1,020 rpm for 10 min (19.1% wt/wt of Sepia melanin ink formulation, Table 1). The mixture was then transferred into an attritor (consisting of a high-rotation speed disk and 900 g of 1 mm diameter zirconium oxide beads in a water-cooled vessel) and continuously mixed for 24 h (2,750 rpm, total applied energy of ∼10.7 kWh) to reduce the size of the agglomerated Sepia melanin particles in the powder state. The final ink was obtained by adding 26 g (4.4% wt/wt) of 1-methoxy-2-propanol and 1.5 g (0.3% wt/wt) of a polyether siloxane copolymer-based additive (TEGO Wet KL 245, Table 1). Proof of printability of our ink was given using the flexographic printing method (Flexiproof 100, laboratory flexographic printer). The ink was deposited onto an anilox roller consisting of engraved cells of 15 billion cubic microns per square inch of surface. The ink was then transferred to a polymer-printing plate and subsequently to an impression cylinder with the substrate (125 μm thick PET and Kromekote paper (Fig. 1 and *SI Appendix*, Movie S1).

The ink was also spin-coated (6,000 rpm, 500 rpm/s, 40 s) on Au-patterned SiO_2/Si for electrical characterization, on fused silica and BaF_2 for UV-Vis and FT-IR spectroscopy, respectively. SiO_2/Si substrates were purchased from Wafer ProTM (thickness, 500 ± 25 μm). SiO_2 was wet-thermally grown and had a thickness of 200 ± 10 nm. As-received wafers were cleaned using sequential sonication baths in acetone (10 min), isopropyl alcohol (10 min), and DI water (10 min), followed by 15 min exposure to UV ozone (Jelight Company, Model 30).

Photolithography: Wafers Patterning. A positive photoresist (AZ900MIR) was deposited by spin-coating on precleaned SiO_2/Si substrates (4,000 rpm, 30 s). Substrates were then soft-baked on a hot plate for 90 s at 90 °C. The pattern mask (planar electrodes with interelectrode distance L= 10 μm, electrode width W= 4 mm, total in-plane area A = 4×10^{-4} cm^2 (Figs. 3*A* and 4*A*, *Insets*) was then placed in a mask aligner (MA6 SUSS Microtec Aligner) to expose the photoresist to UV light (in contact mode [soft vacuum], exposure time 10 s, 57 mJ cm^{-2}). The substrates were then baked for 90 s at 110 °C. The development of the photoresist was performed by immerging the substrates in a developer solvent (AZ726) and gently stirring for 60 s. The substrates were finally washed with DI water and dried with a nitrogen gun.

Electrode Deposition. Patterned wafers were placed in an electron-beam evaporation chamber (10^{-6} Torr) for the deposition of gold (Au) electrodes. The thickness of the metal layers was controlled with a quartz-microbalance. The deposition of the 5 nm-thick titanium (Ti) adhesion layer was followed by the deposition of 40 nm-thick Au on the substrate (deposition rate 0.7 Å s^{-1}). Then, lift-off was performed (Microposit 1165, heated at 70 °C for 2 h and rested for 24 h in the photoresist remover, washed with DI water, and dried with nitrogen gun). SiO_2/Si wafers patterned with Au electrodes were then diced into 1 cm × 1 cm. Prior to the deposition of the Sepia melanin ink, substrates were cleaned as for the prepatterning cleaning process. Scotch tape was used to avoid coating the electrodes pad by the deposition of the Sepia melanin films by spin-coating. After the deposition, the scotch tape was carefully removed, and the pads were cleaned with an IPA-damped cotton swab and dried with a nitrogen gun.

Morphology. The morphology of Sepia melanin films was investigated on 1 cm × 1 cm SiO_2/Si and 3 cm × 3 cm Kromekote paper by SEM (JEOL JSM7600F microscope, backscattering mode, voltage 1 kV and 5 kV) and AFM in tapping mode (AFM Bruker FAST SCAN ICON microscope, aluminum-coated silicon cantilever [tip radius 10 nm, spring constant 42 N m^{-1}]).

Thickness. Sepia melanin film thickness was measured on SiO_2/Si and PET using a stylus profilometer (DekTak kXT, Bruker, 10 nm height resolution) coupled to the *Vision64* software.

UV-Vis-NIR Absorption Spectroscopy. UV-Vis-NIR spectra of spin-coated Sepia melanin films were collected on fused silica (JGS1 glass, thickness 1 mm, diameter 12 mm, Changchun Yutai Optics Co., Ltd.) using a Cary 7000 Universal Measurements Spectrophotometer (Agilent UMS) equipped with an integrating sphere (Labsphere). This setup allowed for the simultaneous measurements of reflected (R) and transmitted (T) radiation in the 250–1,000 nm range. The total optical film absorption (A) was evaluated as $A = 1 - T - R$.

Electrical Characterization. Sepia melanin films were deposited by (1) spin-coating onto 1 cm × 1 cm SiO_2/Si photolithographically patterned with planar Au electrodes (5 nm Ti adhesion layer, 40 nm of Au, with interelectrode distance L= 10 μm, electrode width W= 4 mm, total in-plane area A = 4×10^{-4} cm^2) (Figs. 3*A* and 4*A*, *Insets*); (2) flexography onto 125-μm-thick PET patterned with interdigitated Ag electrodes (electrode thickness, 325 nm; electrode width, W = 2 cm; interelectrode distances, L_1 = 100 μm, L_2 = 150 μm, L_3 = 500 μm, and L_4 = 750 μm; corresponding to in-plane areas, $A_1 = 2 \times 10^{-2}$ cm^2, $A_2 = 3 \times 10^{-2}$ cm^2, $A_3 = 5 \times 10^{-2}$ cm^2, and $A_4 = 3 \times 10^{-1}$ cm^2, respectively) (Fig. 3*B*, *Inset*). Ag electrodes featuring electrical conductivity of 4.4×10^6 S m^{-1} were deposited via roll-to-roll press with flexography printing units (OMET, Varyflex V2) using a water-based nano-silver ink (NovaCentrix, PFI600) (56, 57).

I–V measurements were acquired at ambient conditions on (1) spin-coated films on 1 cm × 1 cm Au-patterned SiO_2/Si electrodes, and (2) printed films on PET and paper patterned with interdigitated Ag flexographically printed electrodes using Agilent B1500 semiconductor analyzer.

Temperature-dependent electrical response of spin-coated Sepia melanin films was acquired in vacuum on 1 cm × 1 cm Au-patterned SiO_2/Si planar electrodes in a cryogenic micromanipulated optoelectronic probe station (CPX Lakeshore) equipped with a heating stage (10^{-7} Torr, from 265 K to 325 K at steps of 10 K).

The electrical conductivity of Sepia melanin films was evaluated from the temperature-dependent I–V response as follows

$$\sigma = \frac{L}{A * R}, \quad (1)$$

where R is the film resistance (including the contact resistance) measured at an applied voltage V = 10 V (*SI Appendix*, Table S6) and A is the cross-sectional area.

The electrical conductivity of Sepia melanin films was also evaluated on square substrates (1 cm × 1 cm) using a four-point probe system (Jandel Engineering Ltd.; probe spacing, 1 mm) connected to a source measure unit (SMU, Keysight B2902A, voltage range from 0 V to 1 V). The four-point probe electrical conductivity was measured at RT in the voltage range 0–1 V and computed as follows

$$\sigma = [4.53 \times R_{sh} \times t]^{-1}, \quad (2)$$

where R_{sh} and t are the sheet resistance and film thickness, respectively. Prior to the acquisition, the system was calibrated using an Indium Titanium Oxide (ITO) reference sample (Jandel Engineering Ltd., sheet resistance 13.07 Ω per square inch).

IS. IS data were collected at open circuit potential in the frequency range 3 MHz–1 Hz (20 points per decade, 10 mV oscillation amplitude) using a multichannel potentiostat (Biologic, model VSP 300).

NAA. NAA analysis of Sepia melanin powders, ink and spin-coated films was carried out with the SLOWPOKE nuclear reactor available at Polytechnique Montreal (irradiation time, 600 s; average neutron flux of 5×10^{11} neutrons per cm^2 s^{-1}; analysis chamber equipped with a germanium semiconductor γ-ray detector [Ortec, GEM55185]).

Infrared Spectroscopy. FT-IR of spin-coated Sepia melanin films were acquired on BaF_2 (ThorLabs; thickness, 3 mm; diameter, 12.7 mm) in inert atmosphere and in transmission mode using Vertex 70 FT-IR spectrometer (Bruker Optics) equipped with a DLaTGS detector. IR spectra were collected at a resolution of 4 cm^{-1} by averaging 200 scans.

Raman Spectroscopy. Raman spectra of spin-coated Sepia melanin films were acquired on SiO_2/Si using a Renishaw inVia Raman spectrometer (λ = 514 nm; wavelength scan rate, 100 nm s^{-1}; 5% of total power to prevent film overheating).

XPS. XPS analysis of Sepia melanin powders and films spin-coated on SiO_2/Si was carried out with a VG Escalab 222i XL apparatus (source monochromatic Kα [1486.6 eV]; X-ray beam size, 0.75 mm × 1 mm; power, 150 W [10 kV, 15 mA]; pressure in analysis chamber, ≤10^{-9} Torr; probed area, 1 mm^2; depth of analysis, ≤10 nm; detection limit, 0.1% at). Ten survey scans were carried out from 0 eV to 1,300 eV at steps of 1 eV (pass energy, 100 eV; dwell time,

100 ms). Background subtraction was performed via the Shirley method, and peak positions were referenced to C_{1s} at 285 eV.

Data Availability. All study data are included in the article and/or the *SI Appendix*.

ACKNOWLEDGMENTS. The authors thank A. Carrière, D. Lacombe, D. Niyonkuru, and R. Karimi Azari for their support during the extraction and purification of Sepia melanin powders. The authors are grateful to Dr. G. De Crescenzo and Dr. B. Liberelle for the lyophilization of Sepia melanin powders. Dr. S. Elouatik (Raman Spectroscopy), Dr. C. Chebanier (XPS), Dr. C. Pellerin (FT-IR), Dr. C. Chilian (NAA), O. Girard (SEM), P. Moraille (AFM), and Y. Drolet are gratefully acknowledged for technical support and critical insights. The authors are thankful to Dr. A. Saucier, Dr. A. Yelon, Dr. T. Szkopek, P.-J. Alarco, and Dr. A. Gouda for fruitful scientific discussions and to the director of the Printability and Graphic Communications Institute (ICI, Montréal), Dr. Chloe Bois.

Author affiliations: [a]Engineering Physics Department, Polytechnique Montréal, Montréal, QC H3T 1J4, Canada; [b]Printability and Graphic Communication Institute, Montréal, QC H2M 2E2, Canada; and [c]Department of Chemistry "Giacomo Ciamician", Alma Mater Studiorum, Università di Bologna, Bologna 40126, Italy

1. C. Bee *et al.*, Molecular-level similarity search brings computing to DNA data storage. *Nat. Commun.* **12**, 4764 (2021).
2. N. Armaroli, V. Balzani, Solar electricity and solar fuels: Status and perspectives in the context of the energy transition. *Chemistry* **22**, 32–57 (2016).
3. V. Forti, C. P. Baldé, R. Kuehr, G. Bel, *The Global E-waste Monitor 2020: Quantities Flows, and the Circular Economy Potential* (United Nations University/United Nations Institute for Training and Research, International Telecommunication Union, and International Solid Waste Association, 2020).
4. A. Gouda *et al.*, "Biodegradability and compostability aspects of organic electronics materials and devices" in *Electronic Waste: Recycling and Reprocessing for a Sustainable Future*, M. E. Holuszko, A. Kumar, D. C. R. Espinosa, Eds. (Wiley-VCH, 2021), pp. 255–285.
5. M. Meloni, F. Souchet, D. Sturges, Circular consumer electronics: An initial exploration. *Ellen MacArthur Found.*, 1–17 (2018).
6. M. Irimia-Vladu, "Green" electronics: Biodegradable and biocompatible materials and devices for sustainable future. *Chem. Soc. Rev.* **43**, 588–610 (2014).
7. M. Irimia-Vladu, E. D. Glowacki, N. S. Sariciftci, S. Bauer, *Green Materials for Electronics*, S. B. Irimia-Vladu, Mihai, E. D. Glowacki, N. S. Sariciftci, Eds. (Wiley-VCH, Weinheim, Germany, 2018).
8. A. Nzihou, *Handbook on Characterization of Biomass, BioWaste and Related By-products*, A. Nzihou, Ed. (Springer, 2020).
9. P. Meredith, C. J. Bettinger, M. Irimia-Vladu, A. B. Mostert, P. E. Schwenn, Electronic and optoelectronic materials and devices inspired by nature. *Rep. Prog. Phys.* **76**, 034501–034537 (2013).
10. C. Kittel, *Introduction to Solid State Physics*, S. Johnson, P. McFadden, M. Batey, Eds. (Wiley J. and Sons Inc., 2005).
11. N. W. Ashcroft, N. D. Mermin, *Solid State Physics*, D. Garbose Crane, Ed. (Harcourt College Publishers, 1976).
12. G. Malliaras, R. Friend, An organic electronics primer. *Phys. Today* **58**, 53–58 (2005).
13. H. Shirikawa, Nobel Prize in Chemistry 2000: Electrically conductive plastic the discovery of polyacetylene film: the dawning of an era. *Angew. Chem. Int. Ed.* **40**, 2574–2580 (2001).
14. F. Cicoira, C. Santato, *Organic Electronics: Emerging Concepts and Technologies*, F. Cicoira, C. Santato, Eds. (Wiley-VCH, 2013).
15. I. Mihai, F. Addiégo, D. Del Frari, J. Ô. Bour, V. Ball, Associating oriented polyaniline and eumelanin in a reactive layer-by-layer manner: composites with high electrical conductivity. *Colloids Surf. A Physicochem. Eng. Asp.* **434**, 118–125 (2013).
16. T. Eom *et al.*, Nanoarchitecturing of natural melanin nanospheres by layer-by-layer assembly: Macroscale anti-inflammatory conductive coatings with optoelectronic tunability. *Biomacromolecules* **18**, 1908–1917 (2017).
17. N. Amdursky, E. D. Głowacki, P. Meredith, Macroscale biomolecular electronics and ionics. *Adv. Mater.* **31**, e1802221 (2019).
18. L. Panzella *et al.*, Atypical structural and π-electron features of a melanin polymer that lead to superior free-radical-scavenging properties. *Angew. Chem. Int. Ed. Engl.* **52**, 12684–12687 (2013).
19. M. d'Ischia, A. Napolitano, A. Pezzella, P. Meredith, M. Buehler, Melanin biopolymers: Tailoring chemical complexity for materials design. *Angew. Chem. Int. Ed. Engl.* **59**, 11196–11205 (2020).
20. C. M. R. Clancy, J. D. Simon, Ultrastructural organization of eumelanin from Sepia officinalis measured by atomic force microscopy. *Biochemistry* **40**, 13353–13360 (2001).
21. A. Büngeler, B. Hämisch, O. I. Strube, The supramolecular buildup of eumelanin: Structures, mechanisms, controllability. *Int. J. Mol. Sci.* **18**, 1901–1915 (2017).
22. A. Büngeler, B. Hämisch, K. Huber, W. Bremser, O. I. Strube, Insight into the final step of the supramolecular buildup of eumelanin. *Langmuir* **33**, 6895–6901 (2017).
23. J. Cheng, S. C. Moss, M. Eisner, X-ray characterization of melanins–II. *Pigment Cell Res.* **7**, 263–273 (1994).
24. J. Cheng, S. C. Moss, M. Eisner, P. Zschack, X-ray characterization of melanins–I. *Pigment Cell Res.* **7**, 255–262 (1994).
25. A. Mbonyiryivuze *et al.*, Morphological and chemical composition characterization of commercial sepia melanin. *Am. J. Nanomater.* **3**, 22–27 (2015).
26. J. McGinness, P. Corry, P. Proctor, Amorphous semiconductor switching in melanins. *Science* **183**, 853–855 (1974).
27. M. R. Powell, B. Rosenberg, Nature of the charge carriers in solvated biomacromolecules: DNA and water. *Biopolymers* **9**, 1403–1406 (1970).
28. A. B. Mostert *et al.*, Role of semiconductivity and ion transport in the electrical conduction of melanin. *Proc. Natl. Acad. Sci. U.S.A.* **109**, 8943–8947 (2012).
29. M. Sheliakina, A. B. Mostert, P. Meredith, An all-solid-state biocompatible ion-to-electron transducer for bioelectronics. *Mater. Horiz.* **5**, 256–263 (2018).
30. A. B. Mostert, B. J. Powell, I. R. Gentle, P. Meredith, On the origin of electrical conductivity in the bio-electronic material melanin. *Appl. Phys. Lett.* **100**, 1–3 (2012).
31. A. B. Mostert, S. B. Rienecker, C. Noble, G. R. Hanson, P. Meredith, The photoreactive free radical in eumelanin. *Sci. Adv.* **4**, eaaq1293 (2018).
32. M. Sheliakina, A. B. Mostert, P. Meredith, Decoupling ionic and electronic currents in melanin. *Adv. Funct. Mater.* **28**, 1805514 (2018).
33. A. B. Mostert *et al.*, Gaseous adsorption in melanins: Hydrophilic biomacromolecules with high electrical conductivities. *Langmuir* **26**, 412–416 (2010).
34. M. Reali *et al.*, Electronic transport in the biopigment sepia melanin. *ACS Appl. Bio Mater.* **3**, 5244–5252 (2020).
35. J. Wünsche *et al.*, Protonic and electronic transport in hydrated thin films of the pigment eumelanin. *Chem. Mater.* **27**, 436–442 (2015).
36. M. M. Jastrzebska, H. Isotalo, J. Paloheimo, H. Stubb, Electrical conductivity of synthetic DOPA-melanin polymer for different hydration states and temperatures. *J. Biomater. Sci. Polym. Ed.* **7**, 577–586 (1995).
37. L. Migliaccio *et al.*, Evidence of unprecedented high electronic conductivity in mammalian pigment based eumelanin thin films after thermal annealing in vacuum. *Front Chem.* **7**, 162 (2019).
38. F. M. Smits, Measurement of sheet resistivities with the four-point probe. *Bell Syst. Tech. J.* **37**, 711–718 (1958).
39. J. Wünsche, F. Cicoira, C. F. O. Graeff, C. Santato, Eumelanin thin films: Solution-processing, growth, and charge transport properties. *J. Mater. Chem. B Mater. Biol. Med.* **1**, 3836–3842 (2013).
40. M. Ambrico *et al.*, Hysteresis-type current-voltage characteristics in Au/eumelanin/ITO/glass structure: Towards melanin based memory devices. *Org. Electron.* **11**, 1809–1814 (2010).
41. E. Di Mauro *et al.*, Resistive switching controlled by the hydration level in thin films of the biopigment eumelanin. *J. Mater. Chem. C Mater. Opt. Electron. Devices* **4**, 9544–9553 (2016).
42. M. Reali *et al.*, Eumelanin: From molecular state to film. *J. Phys. Chem. C* **125**, 3567–3576 (2021).
43. R. Noriega *et al.*, A general relationship between disorder, aggregation and charge transport in conjugated polymers. *Nat. Mater.* **12**, 1038–1044 (2013).
44. A. Salleo, "Electronic traps in organic semiconductors" in *Organic Electronics: Emerging Concepts and Technology*, C. Cicoira, F. Santato, Ed. (Wiley-VCH, 2013), pp. 341–373.
45. H. F. Haneef, A. M. Zeidell, O. D. Jurchescu, Charge carrier traps in organic semiconductors: A review on the underlying physics and impact on electronic devices. *J. Mater. Chem. C Mater. Opt. Electron. Devices* **8**, 759–787 (2020).
46. S. Wang *et al.*, Electrochemical impedance spectroscopy. *Natl. Rev.* **41**, 1–21 (2021).
47. R. A. Huggins, Simple method to determine electronic conductivity and ionic components of the conductors in mixed a review. *Ionics (Kiel)* **8**, 300–313 (2002).
48. M. L. Tran, B. J. Powell, P. Meredith, Chemical and structural disorder in eumelanins: A possible explanation for broadband absorbance. *Biophys. J.* **90**, 743–752 (2006).
49. V. Capozzi *et al.*, Raman and optical spectroscopy of eumelanin films. *J. Mol. Struct.* **744–747**, 717–721 (2005).
50. S. A. Centeno, J. Shamir, Surface enhanced Raman scattering (SERS) and FTIR characterization of the sepia melanin pigment used in works of art. *J. Mol. Struct.* **873**, 149–159 (2008).
51. M. L. Roldán, S. A. Centeno, A. Rizzo, An improved methodology for the characterization and identification of sepia in works of art by normal Raman and SERS, complemented by FTIR, Py-GC/MS, and XRF. *J. Raman Spectrosc.* **45**, 1160–1171 (2014).
52. M. Mohammadian-Kohol, M. Asgari, H. R. Shakur, A detailed investigation of the gamma-ray radiation effects on the optical properties of polyvinyl butyral film. *Optik (Stuttg.)* **127**, 7459–7468 (2016).
53. H. Fritzsche, "Switching and Memory in Amorphous Semiconductors" in *Amorphous and Liquid Semiconductors*, J. Tauc, Ed. (Plenum Press, 1974), pp. 313–355.
54. M. Jastrzebska, A. Kocot, L. Tajber, Photoconductivity of synthetic dopa-melanin polymer. *J. Photochem. Photobiol. B* **66**, 201–206 (2002).
55. M. Rahaman *et al.*, A new insight in determining the percolation threshold of electrical conductivity for extrinsically conducting polymer composites through different sigmoidal models. *Polymers (Basel)* **9**, 1–17 (2017).
56. N. Xie, W. Shao, L. Zhen, "Percolation in disordered conductor/insulator composites" in *Advanced Composite Materials: Properties and Applications*, I. Grzegorek, A. T. Leverton, Eds. (De Gruyter Open Poland, 2017), pp. 440–467.
57. M. Magarelli, P. Passamonti, C. Renieri, Purification, characterization and analysis of sepia melanin from commercial sepia ink (*Sepia officinalis*). *CES Med. Vet. Zootec.* **5**, 18–28 (2010).
58. M. Araujo, J. R. Xavier, C. D. Nunes, P. D. Vaz, M. Humanes, Marine sponge melanin: A new source of an old biopolymer. *Struct. Chem.* **23**, 115–122 (2012).
59. E. Di Mauro, D. Rho, C. Santato, Biodegradation of bio-sourced and synthetic organic electronic materials towards green organic electronics. *Nat. Commun.* **12**, 3167 (2021).
60. M. Zhuldybina, X. Ropagnol, C. Bois, R. J. Zednik, F. Blanchard, Printing accuracy tracking with 2D optical microscopy and super-resolution metamaterial-assisted 1D terahertz spectroscopy. npj Flex. *Electron.* **4**, 1–7 (2020).